HIGH RESOLUTION GEOMORPHIC MAP OF MALAPERT MASSIF. W. Iqbal[1], C. H. van der Bogert[1], V. T. Bickel[2], L. Wueller[1], H. Hiesinger[1], D. A. Kring[3],[1]Institut für Planetologie, Universität Münster, Wilhelm-Klemm-Str. 10, 48149 Münster, Germany, (iqbalw@uni-muenster.de), [2]Center for Space and Habitability, University of Bern, CH. [3]Lunar and Planetary Institute, USRA, Houston, TX, USA.

Introduction: The Malapert massif is one of the NASA Artemis candidate landing regions and was studied extensively during the NASA call for Artemis III geology teams [1,2]. The region offers important prerequisites for a landed mission, including constant illumination, suitable slopes, and accessibility to permanently shadowed regions (PSRs). The massif is ~50 km long, and rises 5 km above its base. It has been interpreted as a rim remnant of the South-Pole Aitken (SPA) basin (e.g., [3]). Thus, a landing site there could provide samples of not only highland materials, but also reworked ejecta from the formation of the SPA basin. To aid in planning extravehicular activities (EVAs) and sampling, we produced a high-resolution geomorphic map of the region surrounding a proposed Artemis III landing site [1], and we identified multiple regolith and crater units, as well as boulders and other features.

Methods: We used a Lunar Reconnaissance Orbiter (LRO) [4] Narrow Angle Camera (NAC) image mosaic (0.5m/pixel) [5], LOLA DTM (5 m/px) [6] and Mini-RF S-band data (15 m/px) [7]. The LRO NAC data was majorly provided by LRO SOC team [5,8]. In addition, we used derived DTM and slope maps from the LRO NAC stereo image pairs provided by [9]. The HORUS data [10] were used for the identification of the boulders in the shaded areas.

Our geomorphic mapping approach primarily adheres to the standards set by the Federal Geographic Data Committee (2006) [11] and PlanMap (https://wiki.planmap.eu/display/public/D2.1-public) [12]. The digitization scale of the map is 1:2,000 and print scale is 1:8,000.

Geomorphic map: Our preliminary geomorphic map of the Malapert massif (***Fig. 1***) displays variations in regolith textures, the approximate extents of crater materials, and observable regolith-flow materials on crater walls. In addition, permanently shadowed regions (PSRs) [13] and boulder fields are mapped.

The regolith is mapped based on its texture, morphology, and albedo. The *Regolith 1* unit has a rough and irregular pattern, and it exhibits a high albedo. This unit does not show any prominent slumping/regolith flow. *Regolith 2* has a lower albedo and prominent flow with elongated lobate material. This texture is also known as "elephant's hide texture" (e.g., [14-16]). *Regolith 3* also has low albedo, but unlike *Regolith 2,* has a smooth texture. *Regolith 4* has a higher albedo compared to *Regolith 2* and *Regolith 3* and contains slumping material. The slumps in *Regolith 4* are smaller than

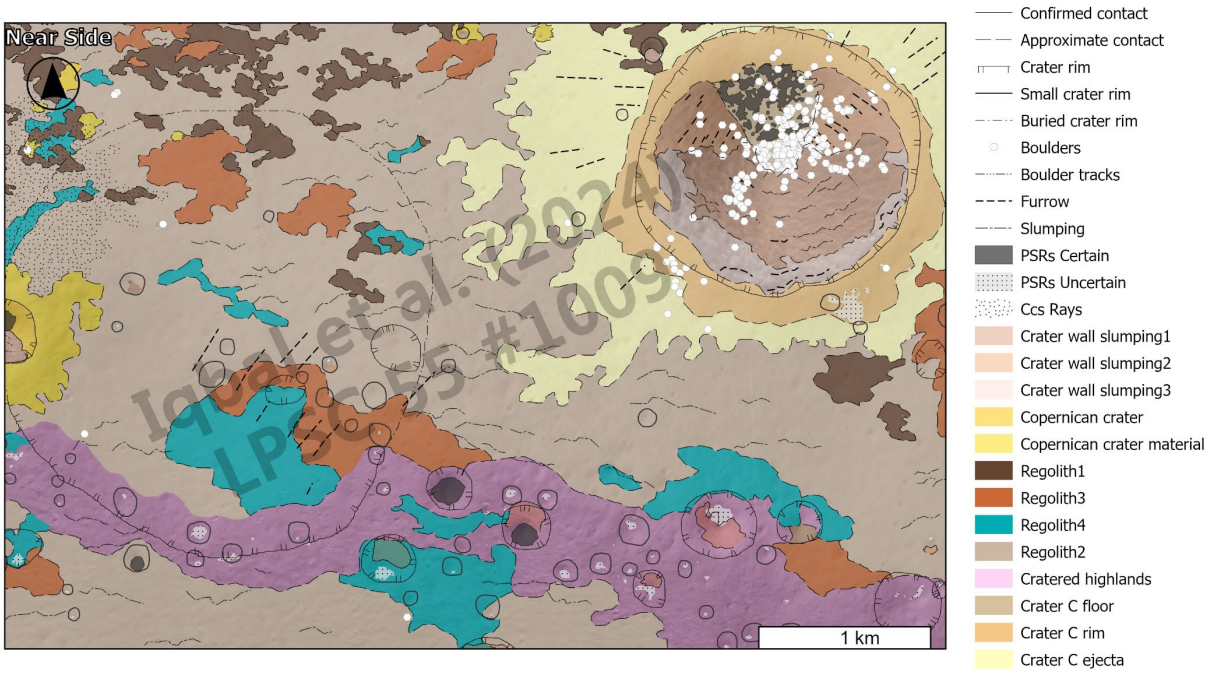

Figure 1. *Preliminary geomorphological map of the region on Malapert massif at the scale 1:8:000.*

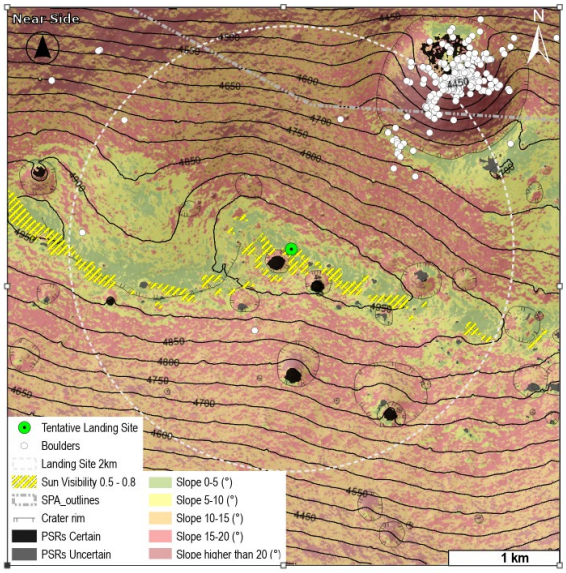

Figure 2. *Variation of slope on Malapert massif along with location of PSRs [13].*

those in *Regolith 2*. At the top of the massif, there is a shallow-sloped region with a high density of craters, which is mapped as *cratered highland*.

A large, young crater with PSR [13] on the near side of the massif is one of the prominent features in the region of interest. Due to its importance for understanding excavated materials that may be sampled during an EVA, we also mapped this crater in detail. Because the crater formed on a steep slope, it exhibits characteristics of oblique craters. For example, the extent of the ejecta greater downhill (towards the near side) compared to uphill. Additionally, the crater has an asymmetrical crater walls. A large boulder field in the crater exhibits the highest boulder concentration on the crater floor offset to the downhill side. A small boulder field was also detected on the uphill rim of the crater.

In addition, we also mapped slumping units observed on the illuminated sides of the crater walls. We mapped three different slumping units: *cws1*, *cws2*, and *cws3*. *Cws1* unit has a chaotic pattern and the lowest albedo compared to *cws2*, and *cws3*. It occurs on slopes > 20° (***Fig. 2***). The unit *cws2* shows furrows and is found on medium slopes. In crater C, the unit *cws2* contains boulder fields. The *cws3* unit is found on steep to moderate slopes and consists of larger blocks of wall and slump material.

Discussion: Due to the accessibility of high resolution data [4-9], we were able to produce a detailed geomorphic map around a potential Artemis III landing site. We observed differences in the regolith, which will provide a basis for exploring the variability of regolith in situ. One factor that may control the regolith textures is local slope (***Fig. 2***). *Regolith 1* is restricted to the slopes greater than 20°. However, composition can be another factor that influences the behavior of the regolith. For example, *Regolith 2* and *Regolith 3* cover regions with both shallow and steep slopes, but *Regolith 2* shows slumping while *Regolith 3* does not. This difference could be due to cohesion differences between regolith types.

Further work: In a continuation of this study, we will perform crater size frequency distribution (CSFD) measurments on different regolith units to test the correlation of regolith texture and slope on crater morphology and spatial density. Understanding the process at the regolith scale will ultimately help us plan safer and more precise landing missions in the future.

Acknowledgements: WI is funded by German Aerospace Agency (DLR) Grant # 50 OO 2102. HH is funded by the German Research Foundation (Deutsche Forschungsgemeinschaft SFB-TRR170, subproject A2) and CvdB is supported by DLR Grant # 50 OW 2001 and the European Union's Horizon 2020 research and innovation programme grant Nº 871149 (Europlanet 2024 RI, GMAP). This contribution is the result of an international collaboration between SSERVI and LPI.

References: [1] Lloyd V. C. et al. (2022) *NASA Release.* 22-089. [2] NASA (2022) *C.24 A3GT*. [3] Garrick-Bethell I. et al. (2009). *Icarus, 204*, 399–408. [4] Robinson M. S. et al. (2010) *Space Sci. Rev., 150,* 81–124 [5] DeRosa D. et al. (2012) *PSS, 74,* 224-226 134 [6] Barker M. K. et al. (2021) *PSS*, *203*, 105119. [7] Fassett C. I. et al. (2023) *LPS LIV,* Abstract #2806. [8] Henriksen M. R. et al. (2023) *SSERVI*, 134. [9] Barker M. K. et al. (2021) *PSS, 203*, 105119. [10] Bickel V. T et al. (2022) *GRL, 49*, e2022GL099530. [11] FGDC (2006) *FGDC-STD-013-2016*. [12] Rothery D. et al. (2018) *PLANMAP,* D2.1-public. [13] Mazarico E. et al. (2011) *Icarus*, *211*,1066–1081. [14] Gold T. (1972) *IAUS 47,* The Moon. 55-67 [15] Zharkova A. Y. et al. (2020) *Icarus*, *351*, 113945. [16] Bernhardt H. et al. (2022) *Icarus*, *379*, 114963.